NASA CR-175008
RSD:86:4101-12-01:01

DEVELOPMENT OF OPTICAL DIAPHRAGM DEFLECTION SENSORS

FINAL REPORT

by

W. L. Ghering, D. Varshneya,
L. A. Jeffers, R. T. Bailey, and J. W. Berthold

THE BABCOCK & WILCOX COMPANY
Research and Development Division

Prepared for

NATIONAL AERONAUTICS AND SPACE ADMINISTRATION
NASA Lewis Research Center
Cleveland, Ohio 44135

Contract NAS3-23712

CONTENTS

LIST OF ILLUSTRATIONS

LIST OF ILLUSTRATIONS (Continued)

LIST OF TABLES

1. SUMMARY

The objective of this project was to develop high-temperature pressure sensors using non-metallic components and optical sensing methods. The sensors were to operate over a temperature range from room temperature (~20°C) to 540°C, to respond to internal pressure up to 690 kPa, to respond to external pressure up to 690 kPa, and to withstand external overpressure of 2070 kPa.

Fused silica was selected as the material for the sensor module on the basis of its high temperature and low thermal expansion characteristics. Optical sensing methods evaluated included the following: microbend, phase sensitive, two-fiber transmission, cantilever slope, and photoelastic. These methods were tested either in the pressure module or under conditions similar to that of the pressure module configuration. Of these sensing methods, the microbend and the phase sensitive sensor were selected for further development and evaluation. These sensors were tested as a function of temperature, pressure, overpressure, and vibration. The microbend sensor (an absolute sensor) exhibited required sensitivity to measure pressure, temperature effects that could be compensated, and insensitivity to vibration; but exhibited a small offset upon overpressurization. The phase sensitive sensor (a relative sensor) exhibited required sensitivity to measure pressure, temperature effects that could be compensated, and insensitivity to vibration and overpressure.

The project results showed that high-temperature pressure sensors based on glass components and optical sensing methods are feasible. The microbend sensor exhibited the required sensitivity and stability to be used as the basis for a compensatable absolute sensor. For the microbend sensor, the 95% confidence level deviation of input pressure from the pressure calculated from the overall temperature-compensated calibration equation was 3.7% of full scale. The limitations of the sensors evaluated were primarily due to the restricted temperature range of suitable commercial available optical fibers and the problems associated with glass-to-metal pressure sealing over the entire testing temperature range.

Glass/ceramic diaphragms and/or optical sensing methods for detecting diaphragm deflection in high-temperature pressure sensors should also be considered for applications such as advanced energy conversion systems, in addition to high-performance aircraft. Such applications with reduced or different design constraints may be directly amenable to solution by state-of-the-art components and sensing methods such as those investigated in this project.

2. INTRODUCTION

Instrumentation for in-flight monitoring of inlet and engine conditions is needed for high-performance aircraft to improve fuel efficiency, engine performance, and overall reliability. This instrumentation must withstand the hostile engine environment which includes the high-temperature operating conditions and vibrations. One of the needed measurements is that of gas path pressure in inlets of engines. In the past, the performance of high-temperature pressure transducers with metallic diaphragms has been limited by creep and hysteresis. One method of eliminating these mechanical and temperature related problems is to employ a non-metallic diaphragm. A further step in this direction would be to employ an optical diaphragm deflection sensing method using non-metallic components such as optical fibers.

The use of optical fibers and optical sensing methods have recently been applied to a number of measurements in hostile environments; these measurements include displacement, velocity, strain, flow, temperature, particle size distribution, gas composition, and fluorescence. These optical sensors can be designed to operate at high temperatures, in regions of high electro-magnetic fields, and other unusual environments.

The scope of this project for high-temperature pressure measurements includes evaluating sensing techniques and sensor systems. These efforts include materials selection, sensing methods, sensor design, sensor fabrication, and sensor testing. The results of this work are applicable to not only the aircraft requirements, but also to similar uses in hostile environments such as advanced energy conversion systems. The information presented is timely in that it reveals the advantages, limitations, and the need for further development of optical sensors and optical components for use in hostile environments.

The purpose of this project was to investigate and develop optical methods to measure diaphragm deflection under hostile conditions. The ultimate objective of

NASA's overall program is to develop pressure transducers capable of operating in a reliable, repeatable fashion to 540°C. The specific objective of this project was to study, design, develop, fabricate, assemble, test, evaluate, and document optical diaphragm deflection sensors that:

- Accurately measure the strain, position, or some other property of diaphragm deflected by a pressure difference across its surface
- Meet the operational and environmental requirements of pressure measurement systems for a high-performance aircraft
- Take full and complete advantage of pertinent current technology in optics, electronics, and materials science

This report describes the pressure sensors that were designed, constructed, and tested in this project. The primary sensors identified were the microbend and the phase sensitive. Two configurations of the microbend are described; the second configuration was to reduce the temperature-induced extraneous sensor response.

Three other sensors that were tested in Phase 1 of the project were the two-fiber transmission, cantilever slope, and photoelastic. These sensors are briefly described.

The description of the sensors is followed by a discussion of the test results. The final section is a summary of results and conclusions.

3. DEVELOPMENT OF MICROBEND SENSOR

The development of the Microbend Optical Diaphragm Deflection Sensor (ODDS) included the sensor module design, the original sensor design, a redesign of the pressure sealing, and the sensor evaluation by a series of specified tests.

3.1 SENSOR DESIGN

The sensor design was based on the objectives of using a non-metallic diaphragm to eliminate or reduce creep and hysteresis, and to meet the requirements and temperature, pressure, and vibrational response. Design constraints included operation to 540°C, response to differential pressure of ±690 kPa full scale, ability to withstand 3X full-scale overpressure, and minimal vibration response from 50 to 2500 Hz.

3.1.1 Design 1

The original sensor design included the basic module design used for all of the sensors, the specific design for the microbend sensing of diaphragm displacement, and the selection of the best available optical fiber.

The basic module design consisted of a fused silica diaphragm optically contacted to a fused silica base plate (see Figure 1). Such a modular construction incorporated the high temperature and low thermal expansion characteristics of fused silica and was inherently vibration resistant. The module design optimized the diaphragm deflection under the constraints of the material tensile strength and the sensor operational specifications. These considerations led to a diaphragm thickness of 5mm, a radius of 20mm, and a deflection of about 2.5 μm at full-scale pressure of 690 kPa. For this diaphragm design, the first normal vibrational mode was >100 kHz.

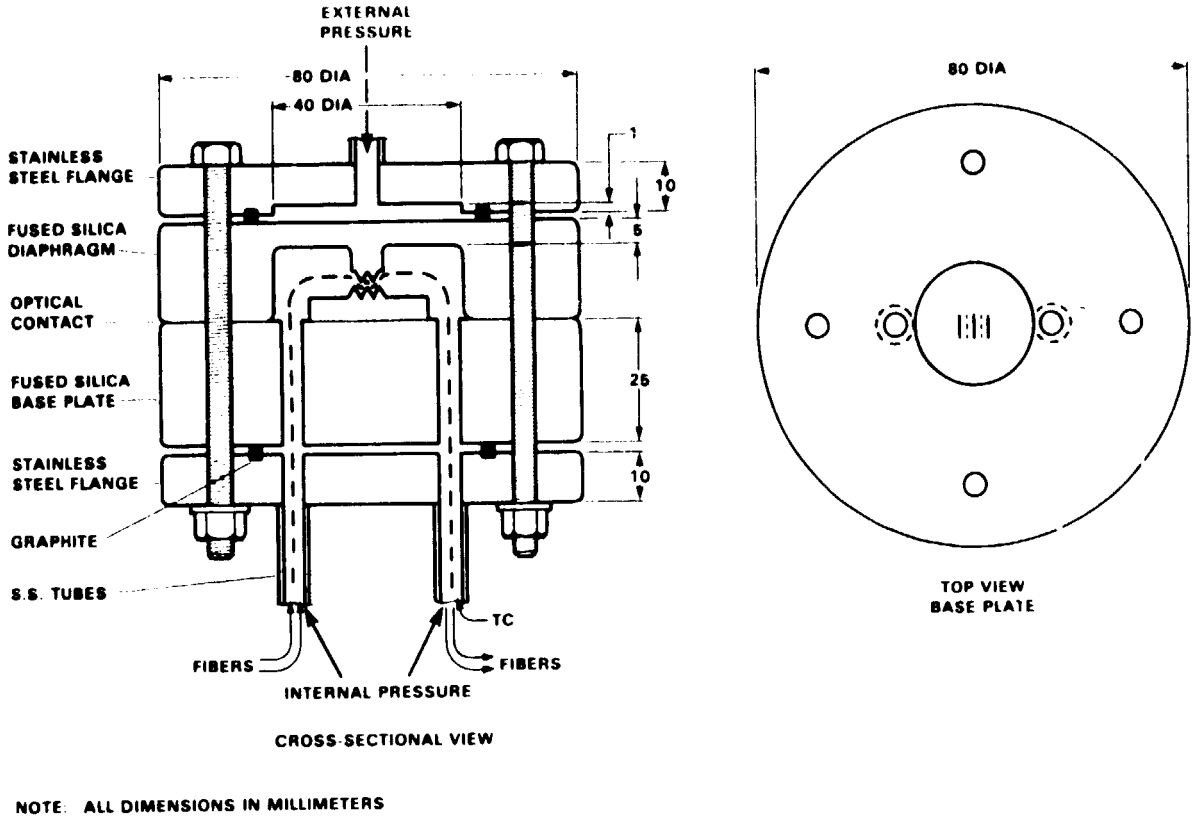

Figure 1. Microbend sensor -- Design 1.

The microbend sensor is based on the attenuation of light transmitted through an optical fiber, the attenuation being caused by a periodic bending of the fiber. The microbend sensor is diagrammed in Figure 1. An optical fiber is squeezed between two sets of corrugations. One set of corrugations is ground along a fused silica block, which is optically contacted to a fused silica base plate. A second set of corrugations is ground along the end of a pedestal located at the center of the diaphragm. The diaphragm is optically contacted to the fused silica base plate around an outer annulus. The optical fiber leads and thermocouples to measure sensor temperature are inserted through holes in the fused silica base plate. The pressure seal between the fused silica module and the positive (external) or negative (internal) pressure is accomplished using graphite gaskets, stainless steel flanges, and flat ($\lambda/10$) optical surfaces. This sealing arrangement replaced the original glass tube seals that were prone to fracture at elevated temperatures. The stainless steel flanges, however, produced an additional thermally-induced response of the sensor; therefore, the flanges were removed in Design 2.

The corrugations on the pedestal are displaced with pressure-induced deflection of the diaphragm. The deflection causes a change in the amplitude of the periodic distortion of the fiber between the corrugations. Optical power in the fiber core is attenuated in proportion to the distortion amplitude via coupling from propagating to radiation modes. The power lost from the core to radiation modes is optimum when the fiber spatial bend frequency equals the difference in propagation constants, $\Delta\beta$, between propagating and radiation modes; shown as:

$$\Delta\beta = \pm \frac{2\pi}{\Lambda}$$

where Λ is the corrugation spacing.

The bend spacing was optimized for an aluminum-coated multimode optical fiber with a core radius of 60 μm and a normalized core clad refractive index difference of 0.003. Both theory and experiment gave an optimum corrugation spacing of ~3mm.

The aluminum-coated fused silica multimode optical fiber was the best available high-temperature fiber for the sensor design and evaluation. This fiber was rugged, and resistant to vibration-induced loss. Also, the fiber exhibited good light transmission properties between 20° and 550°C. However, mechanical degradation of the fiber was noted upon cooling and heat cycling above 450°C.

Compensation for light source changes and changes in the fiber transmission as a function of temperature were accomplished by using a reference fiber (which bypassed the microbend section of the sensor) and a sensor output in terms of the ratio of the difference and sum of the two fiber transmission signals. Compensation for temperature-induced change of the fiber preload would need to be accomplished for a practical pressure transducer using a post processor and the curve fits obtained in the pressure-temperature calibrations.

An exploded view of the microbend sensor with the flanges for pressurization is shown in Figure 2. Details of the microbend diaphragm and the fused silica block optically contacted to the base plate are shown in Figures 3 and 4 (in the second design configuration without bolt holes). Assembly of the sensor provided the required preload on the active fiber for response to the differential pressure of either positive or negative (external or internal) values.

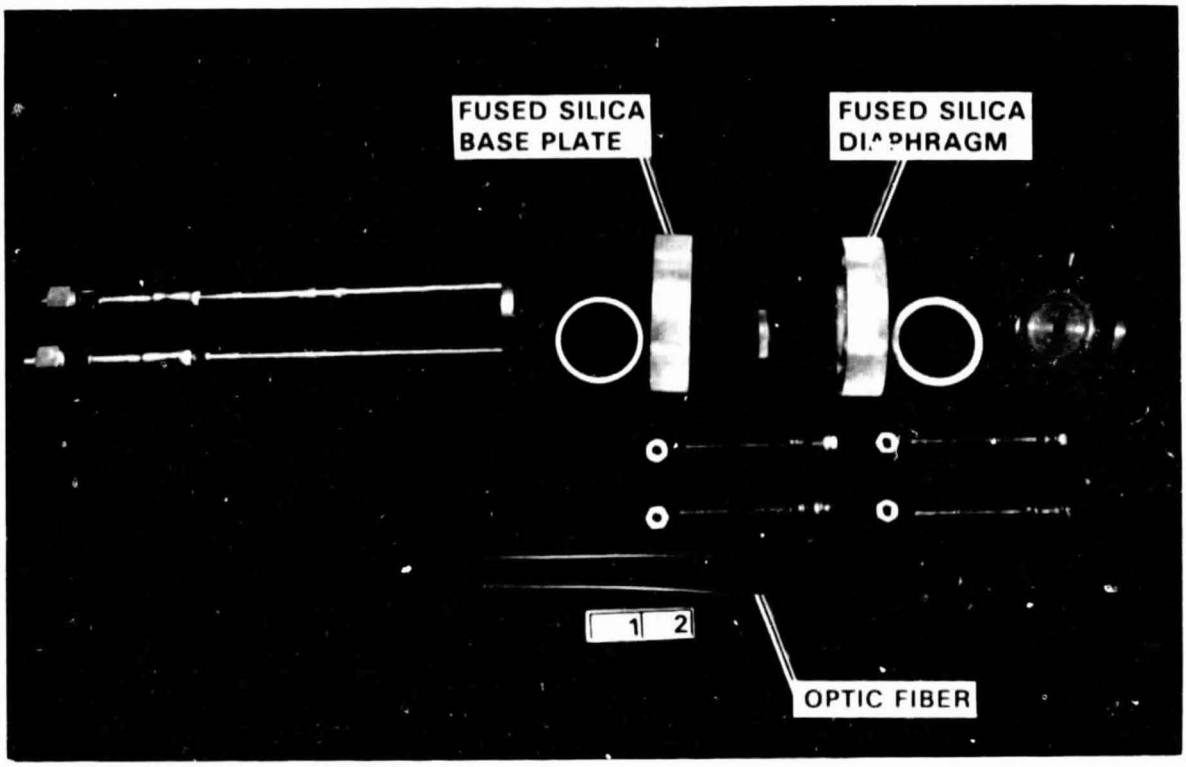

Figure 2. Microbend sensor -- Design 1 exploded view.

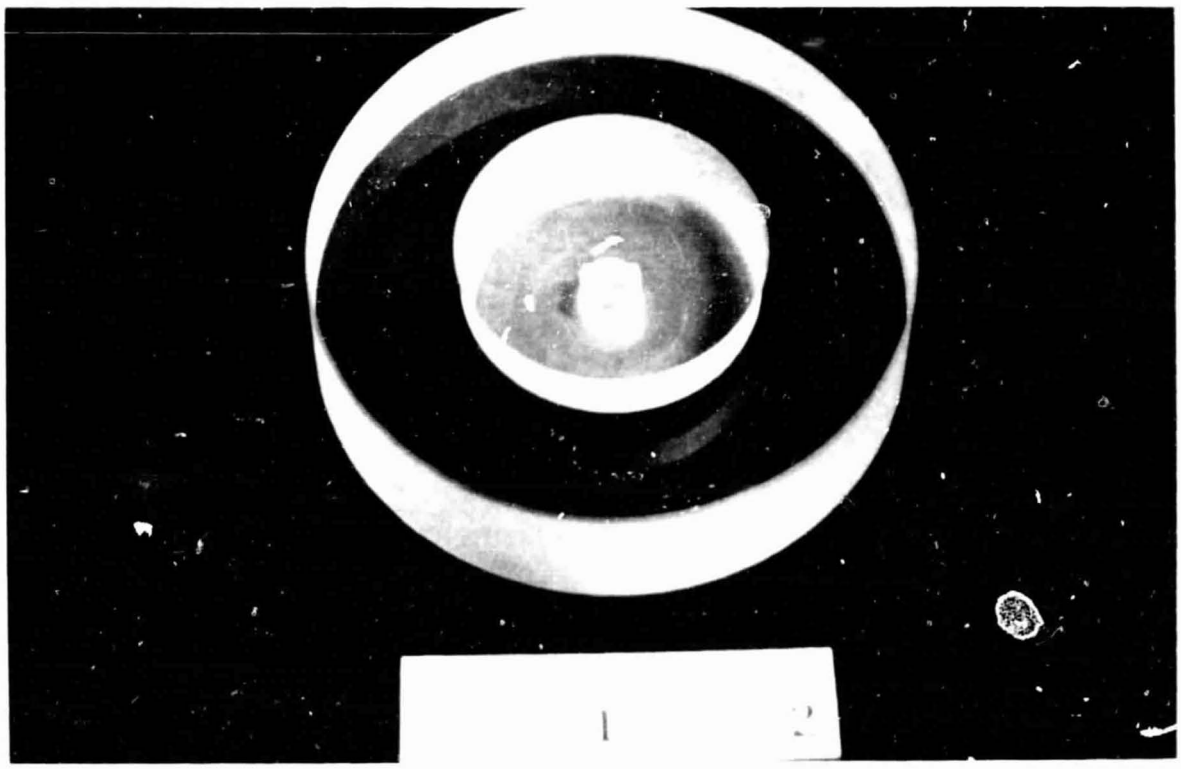

Figure 3. Microbend sensor diaphragm.

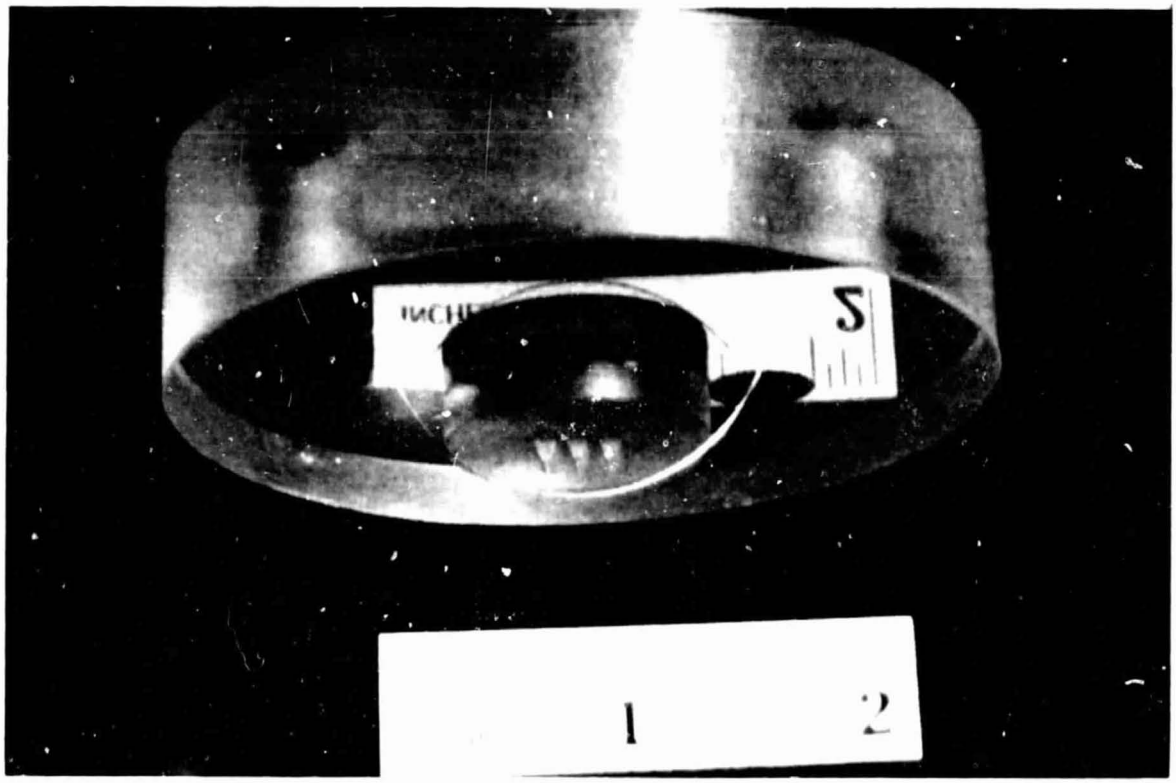

Figure 4. Microbend base plate with fused silica block.

3.1.2 Design 2

The second microbend sensor design still used the basic module components, but incorporated a new pressure sealing arrangement as shown in Figure 5. This pressure sealing arrangement reduced the seal area and thus the thermally-induced stress into the sensor module. This design eliminated most of the sealing-induced diaphragm stress and temperature-induced extraneous sensor response observed during testing of the original design.

An exploded view of the microbend sensor with the modified pressure seal is shown in Figure 6. Assembly of the sensor provides the sealing pressure on the graphite gaskets, and the optical contact between the diaphragm and the fused silica base plate provides the preload on the optical fiber. This assembly is sealed into a pressure chamber at the tube extensions for pressure and temperature testing. For the Design 2 sensor, internal pressure was kept at atmosphere; external pressure was never allowed to go below atmospheric.

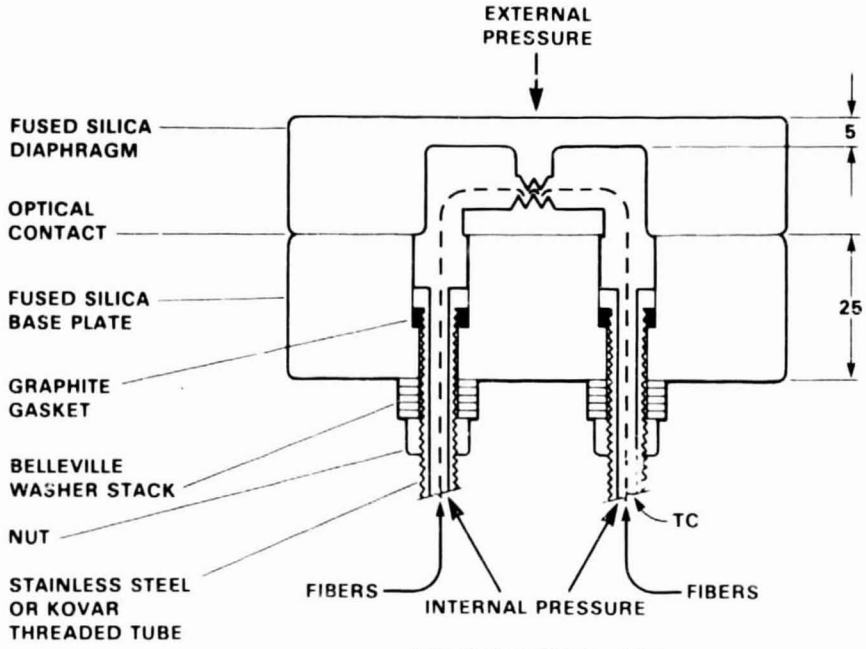

Figure 5. Microbend sensor -- Design 2.

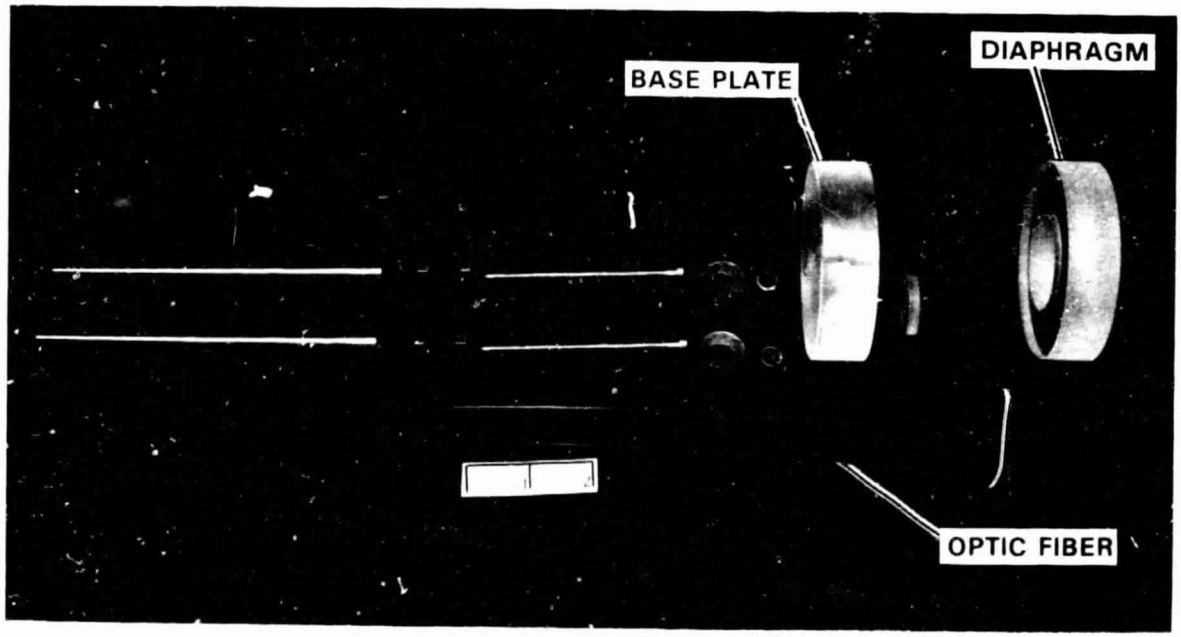

Figure 6. Microbend sensor -- Design 2 exploded view.

3.2 SENSOR EVALUATION

The microbend ODDS was evaluated by a series of specified tests to determine the pressure, temperature, overpressure, and vibration response of the sensor. The sensor evaluation can be summarized as follows:

- Response was approximately linear with pressure from -690 kPa to +690 kPa.
- The sensor exhibited high sensitivity to diaphragm deflection.
- Rapid response to pressure changes.
- The sensor was insensitive to vibration for frequencies of 50 Hz to 2500 Hz.
- The sensor withstood 3X full-scale pressure.
- The sensor module was capable of 540°C operation.
- The best available high-temperature optical fiber produced repeatable response up to about 450°C.
- A small zero offset with temperature was observed for the sensor in the Design 2 configuration.
- The slope of the sensor response with pressure (sensitivity) decreased with an increase in temperature.
- The pressure sealing method for the sensor (Design 1) response characterization produced an additional zero offset with temperature.
- The pressure sealing method for the sensor (Design 1) response characterization produced additional data shifts and scatter.
- The experimental problems experienced with the microbend sensor (Design 1) necessitated the redesign (Design 2) for the subsequent operational and high-temperature tests.
- The microbend sensor (Design 2) test data exhibited the sensitivity and stability as a function of temperature and pressure to be used as the basis for a compensatable sensor.

3.2.1 Operational and High-Temperature Tests for Design 1

The purpose of operational and high-temperature tests were to characterize the sensor response for a sequence of temperatures to 540°C at a sequence of differential pressures from -690 kPa (internal) to +690 kPa (external).

The microbend sensor setup for testing is shown in Figure 7. The output from a LED is split into two parts by a 3 dB coupler and coupled into the aluminum-coated, high-temperature, multimode optical fibers. The fiber output signals are generated by a dual photodetector and associated output circuits. The signals (A, B) are digitized and converted to the form (A - B) / (A + B) for the compensated sensor signal.

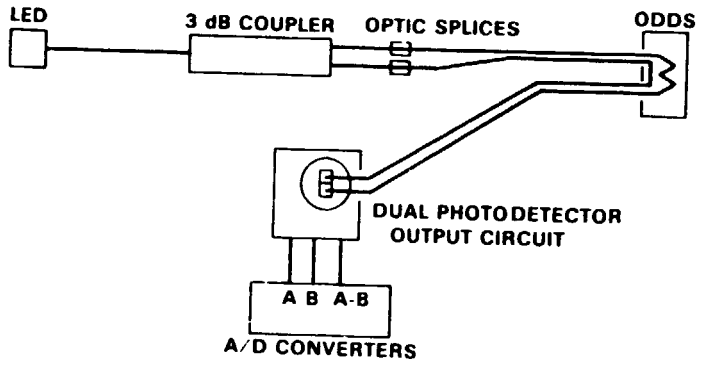

Figure 7. Microbend sensor system block diagram.

A schematic diagram of the test setup is shown in Figure 8 for the microbend sensor. This setup used end plates for pressure sealing. Compressed air was used for the internal and external pressurization. The sensor temperature was controlled by resistance heaters in the laboratory electric furnace. The sensor signals, the calibrated pressure signal, and the calibrated temperature signal were processed by a conventional digital data acquisition system where the experimental results were recorded on floppy disc and also printed after each run. The data was subsequently fitted to a third order polynomial equation of the form:

$$P(T_i) = a_0 + a_1 x + a_2 x^2 + a_3 x^3$$

where:

$P(T_i)$ is pressure at temperature (T_i)

x is sensor output signal

a_0, a_1, a_2, and a_3 are constants for a given temperature

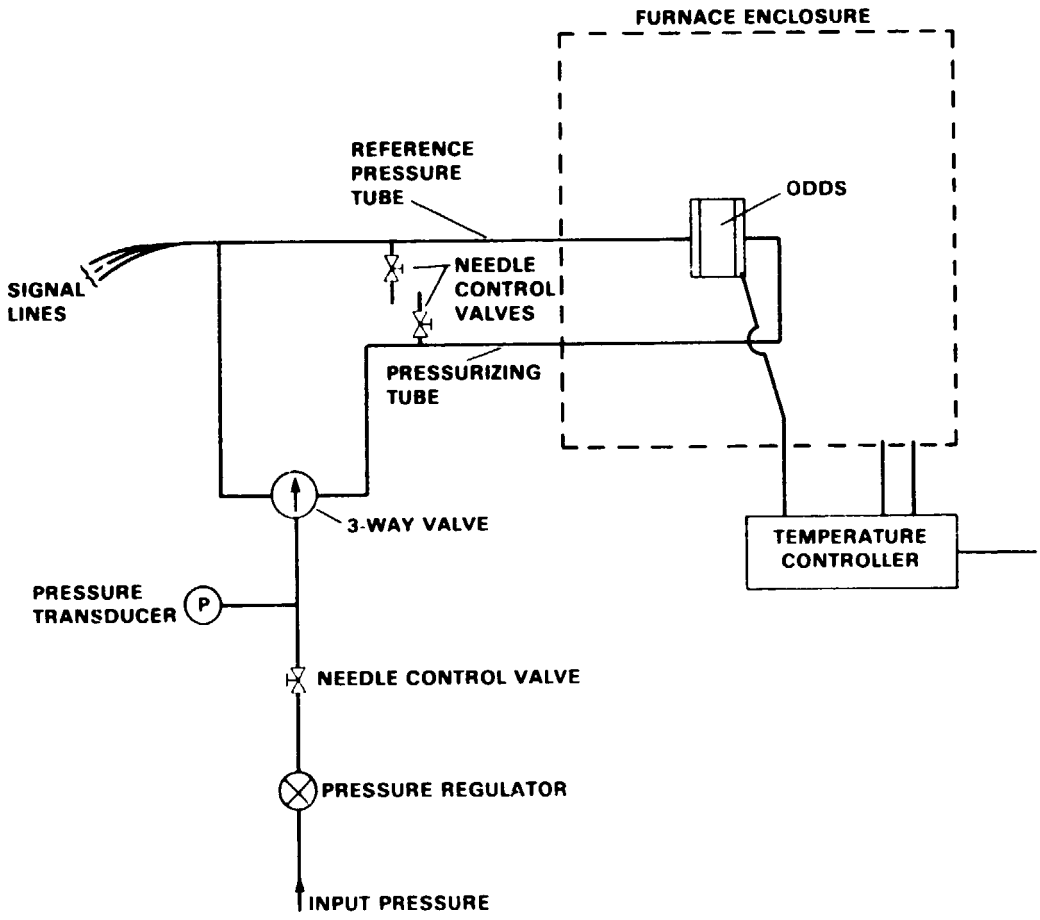

Figure 8. Test setup schematic diagram.

The initial operational and high-temperature test data showed an unexpected zero pressure response shift with temperature and excessive data scatter. This abnormal zero pressure shift was subsequently traced to the pressure sealing method with the stainless steel end plates and graphite gaskets. Although the pressure sealing method of Design 1 introduced spurious sensor response with temperature, the end plates facilitated the testing and avoided the necessity for an optical contact or bonding of the fused silica module. Further, once the spurious effects were characterized, the experimental data could be corrected for the additional zero shift. However, the Design 1 data could not be corrected for the additional data scatter.

Typical microbend response data for the Design 1 configuration is shown in Table 1 and Figure 9. The sensor response at a given temperature was approximately linear with pressure from -690 kPa to +690 kPa. The sensor electronics sensitivity was about 0.56 kPa per bit giving a pressure sensitivity of about 0.08% of full scale. The deflection sensitivity, based on the design deflection of 2.5 μm for full-scale pressure, was about 2 nm. The change in slope of the sensor response to pressure (sensitivity) with a change in temperature was noted for the microbend Design 1 data. Part of this change was attributed to the pressure sealing method which changed the preload on the sensor; an additional part was attributed to the change in the diaphragm stiffness as a function of temperature. The change in the sensor zero response as a function of temperature due to the pressure sealing method can be corrected by using the observed zero shift of about 0.1 full-scale response per 100°C temperature change for the unclamped module. The corrected zero response is shown in Figure 9. The 95% confidence level deviation of the input pressure from the pressure calculated from the individual calibration equations is shown in Table 1. This data shows an increasing error as a function of temperature. The zero shifts and data scatter in the higher temperature runs were partly attributed to the pressure sealing method; this observation was confirmed by additional characterization tests. The experimental problems experienced with the microbend sensor (Design 1) necessitated the redesign (Design 2) for the subsequent operational and high-temperature sensor system tests.

Table 1

MICROBEND SENSOR RESPONSE -- DESIGN 1

Run No.	Nominal Temperature	Full-Scale Error
T1	24°C	1.8%
T2	130°C	8.8%
T3	230°C	14.4%
T4	330°C	19.6%
T5	450°C	34.5%

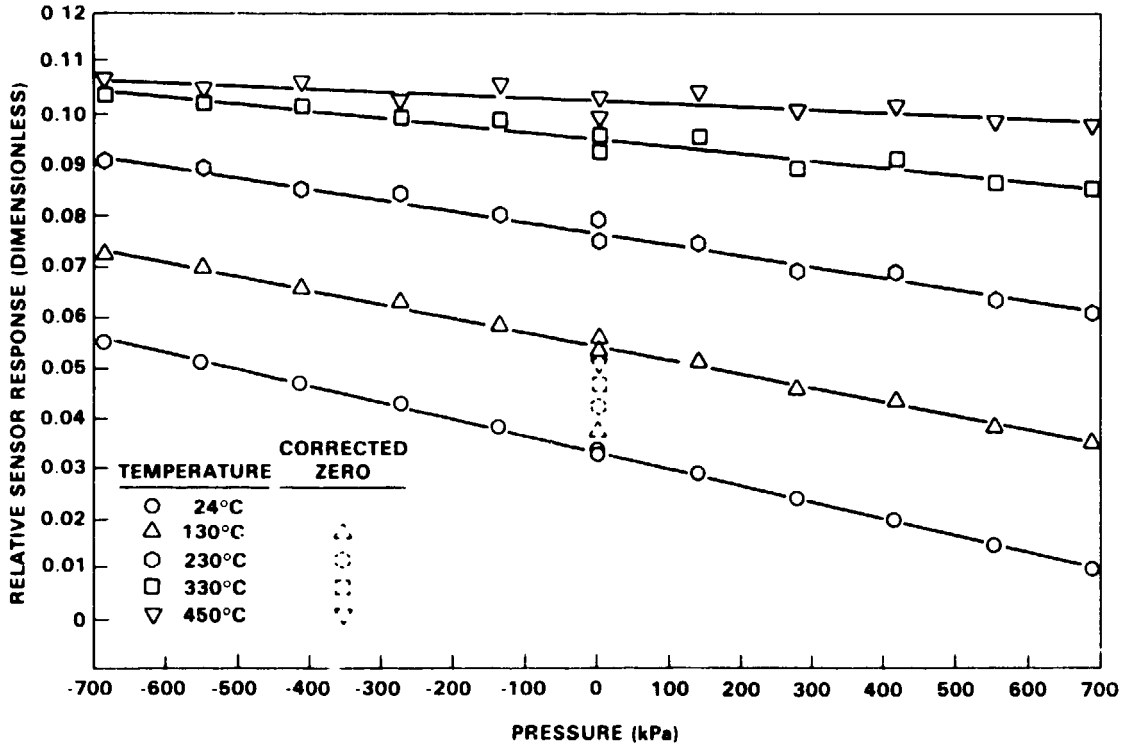

Figure 9. Typical microbend sensor response data for Design 1.

3.2.2 Vibration Test for Design 1

The vibration test objective was to observe and record any mechanical resonances associated with the sensing device. The vibration tests were conducted at room temperature and at zero differential pressure. The sensing device was mounted to a shaker with a suitable fixture with clamping rings and subjected to a sweep frequency sine wave vibration. The sensing device was tested with respect to three mutually perpendicular planes, one of which was the plane of the diaphragm. The vibration amplitude was adjusted such that the mean value of the sensor peak velocity was maintained above a value of 12.7 $x10^{-3}$ m/second (0.5 inch/second) for the frequency range of 50 to 2500 Hz. The duration of the frequency sweep was sufficiently slow to observe and record any mechanical resonances of the sensing device. The sensor was activated during the test with the sensor output signal, V_{out}, recorded as a function of frequency. As shown in Figure 10, V_{out} is determined using the input signals A, B, and A - B from the photodetector output circuit (see Figure 7). The sum signal A + B is obtained from LF356, and AD535 is used to calculate the real-time ratio 10(A - B / A + B) which is recorded as V_{out}.

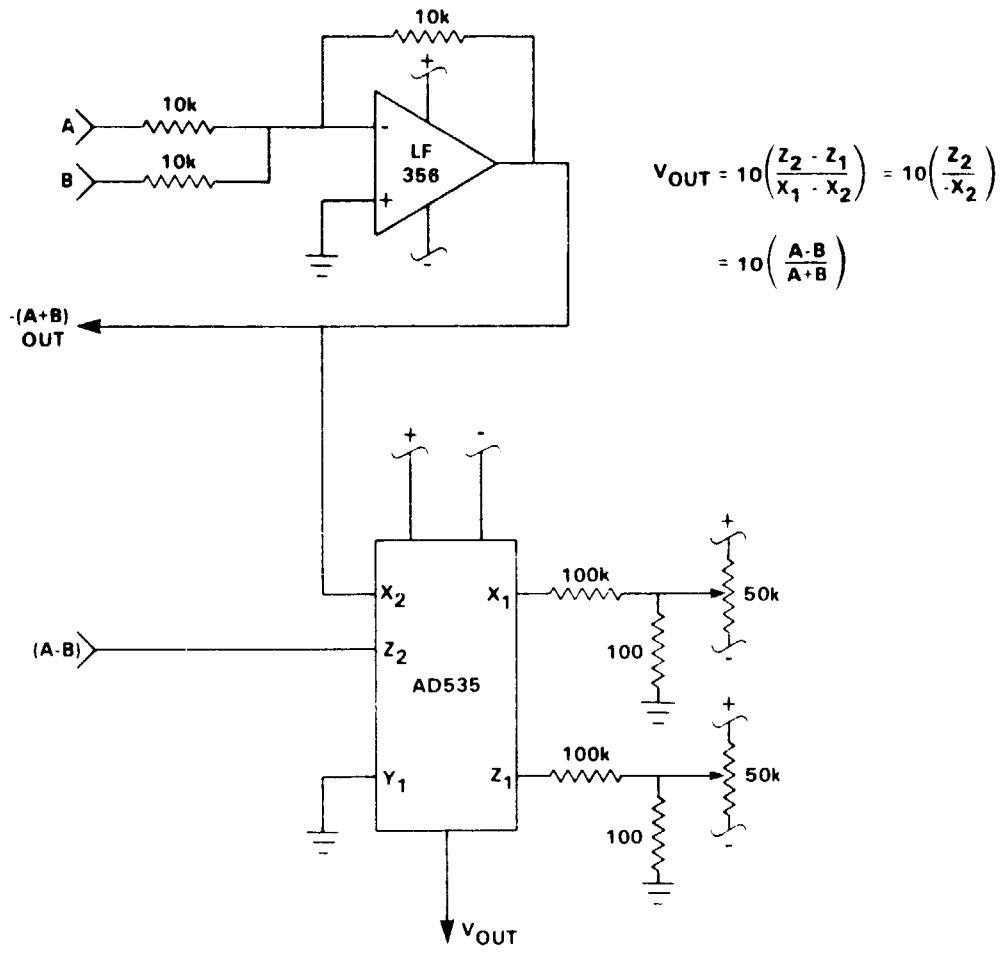

Figure 10. Electronic circuit for microbend sensor vibration test.

A block diagram of the test setup and instrumentation is shown in Figure 11. The test results were recorded on an x-y-y recorder. Typical test results are shown in Figure 12 where the sensor response versus frequency was plotted along with the sensor acceleration level. For all the tests, the sensor (sensing device with activated optical fibers) response was less than 1/4% full-scale pressure response. Therefore, the sensor was found to have no significant resonances and was considered to be essentially immune to vibration over the frequency range of the tests.

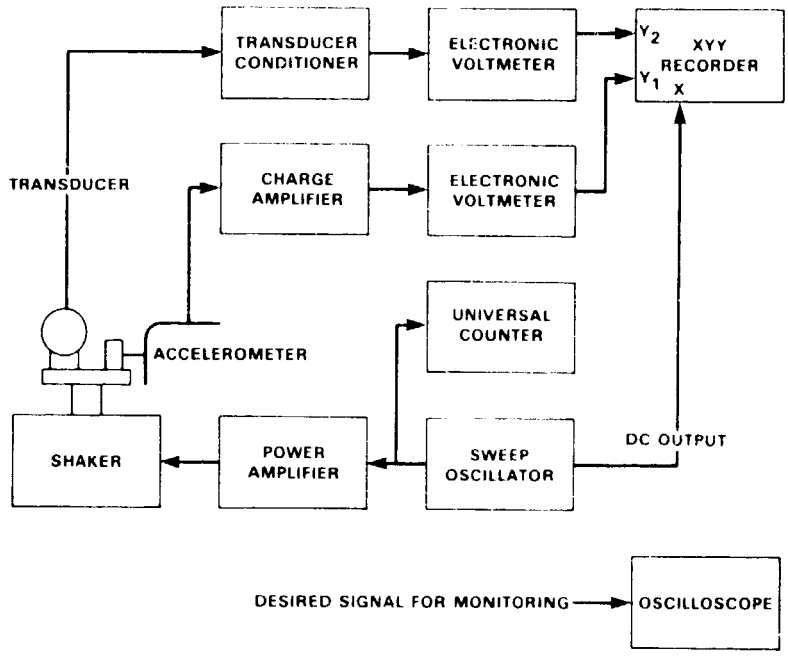

Figure 11. Instrumentation for vibration results.

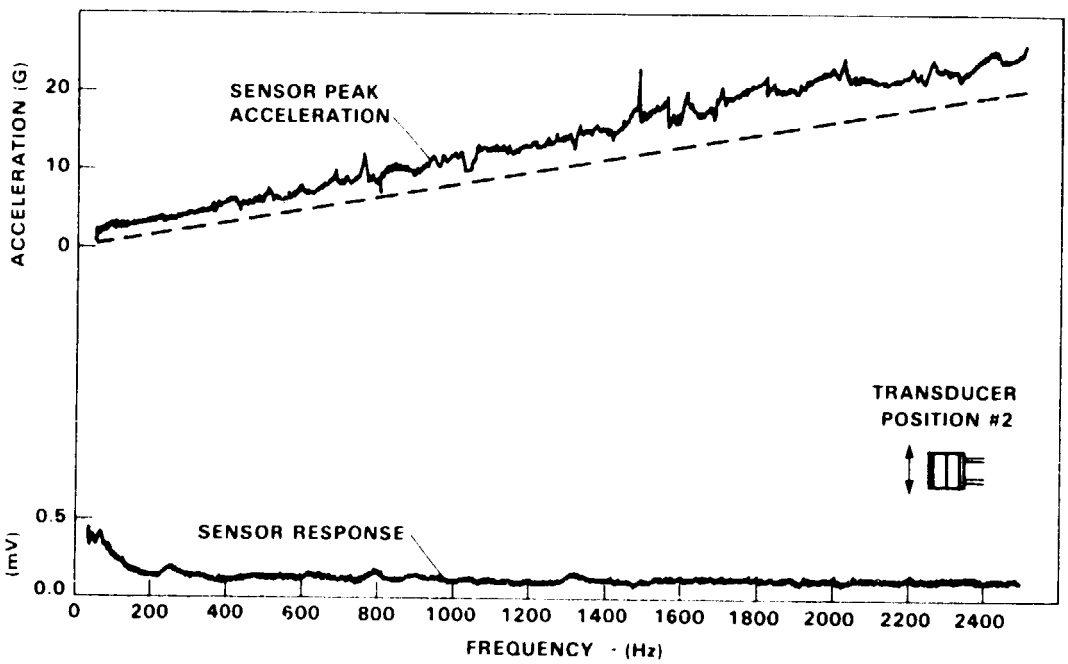

Figure 12. Typical microbend sensor vibration results.

3.2.3 Overpressure Tests for Design 1

The overpressure tests were to verify that the microbend sensor would withstand three times the full-scale pressure without failure and to determine any changes in the sensor response with respect to a baseline calibration equation.

The overpressure tests were conducted at room temperature. The microbend sensing device was subjected to a series of calibration runs alternating with overpressure excursions. The calibration runs after each overpressure excursion were from minus to plus full-scale pressure. The test setup, shown previously in Figure 8, was modified to provide the overpressure excursion as well as to provide control of the calibration runs.

For each static calibration, the 95% confidence level deviation of the input pressure from the pressure calculated from the calibration equation from a baseline static calibration was obtained as a percentage of full-scale pressure. The results of the overpressure test sequence are shown in Figures 13 and 14. Figure 13 shows the raw sensor data versus pressure as a function of the calibration run number. A shift in the sensor response was noted as a function of the run number.

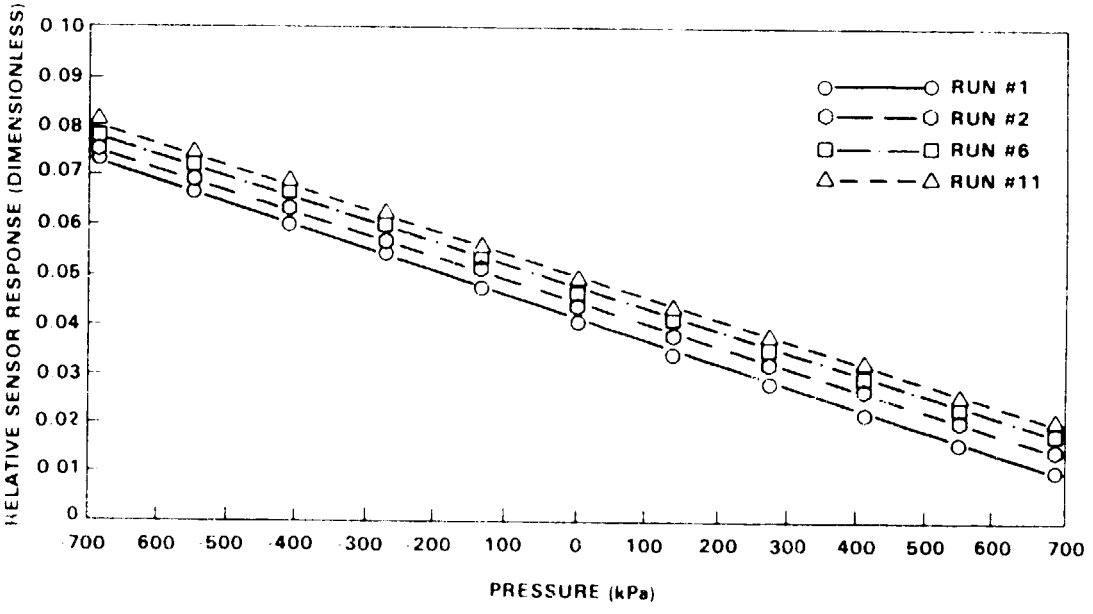

Figure 13. Microbend sensor response during overpressure test sequence.

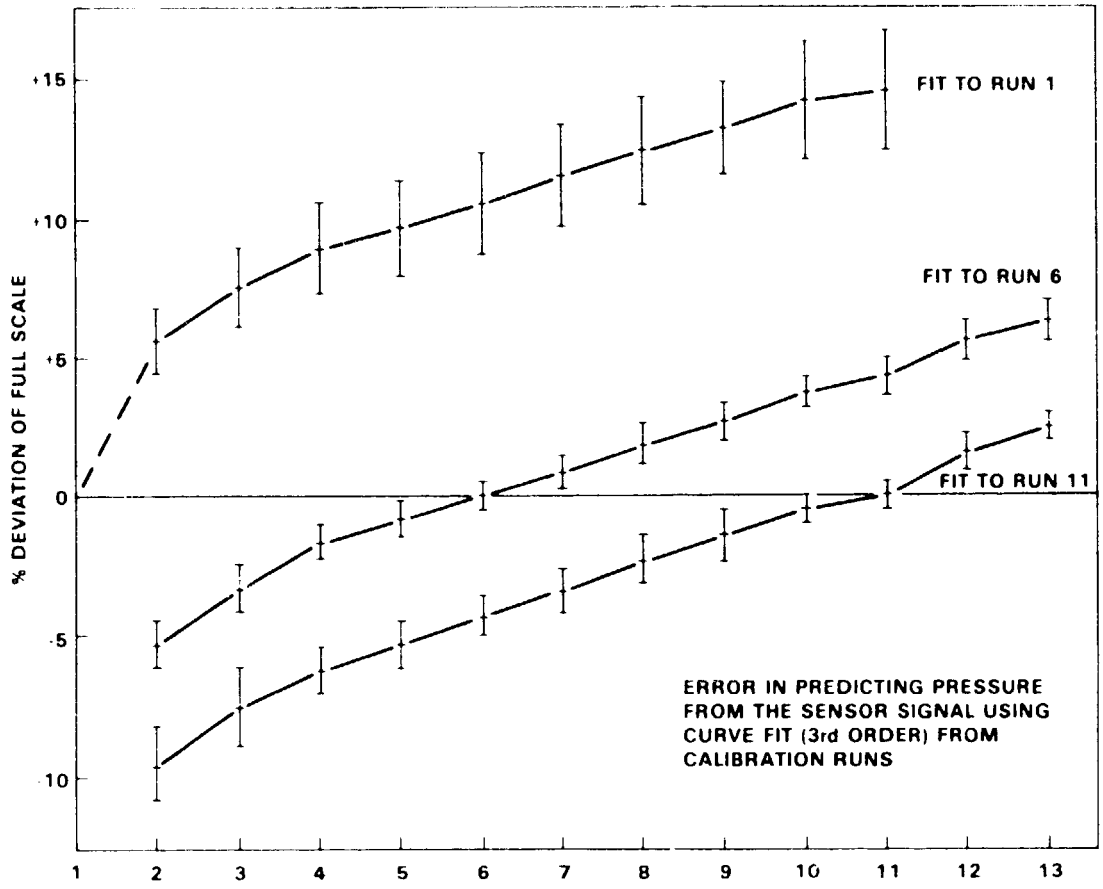

Figure 14. Analysis of microbend sensor response during overpressure test sequence.

This effect is also shown in Figure 14 as the error (in percent deviation of full scale) in predicting the pressure from the sensor signal using the third order curve fit from a calibration run. The comparison is shown using three calibration equations for the prediction. These figures show that each overpressure excursion causes an offset in the sensor response. The first overpressure caused about a 5% offset, each additional overpressure excursion caused about a 1% offset.

3.2.4 Operational and High-Temperature Tests for Design 2

The operational and high-temperature tests for the Design 2 microbend sensor were to characterize the sensor response for a limited sequence of temperatures to

420°C and external pressures to 690 kPa. The Design 2 microbend sensor is shown in Figure 5. The sensor system and test setup were similar to the Design 1 tests shown earlier in Figures 7 and 8; the major difference being that the pressure sealing area had been substantially reduced. The sensor was placed in a pressure chamber (shown in Figure 15) which was located in the furnace enclosure for testing at high temperatures.

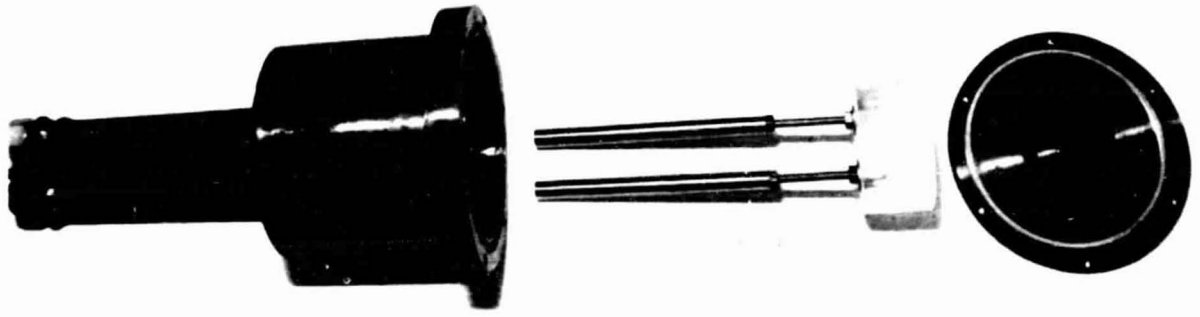

Figure 15. Design 2 microbend sensor with pressure chamber.

The sensor signals, the calibrated pressure signal, and the calibrated temperature signal were processed by a conventional digital data acquisition system. The data was subsequently fitted to third-order polynomial equations to predict pressure from the sensor signal at a given temperature (refer to Section 3.2.1). The data was also fitted to an overall temperature compensated calibration equation given by:

$$P = c_1 + c_2 T + c_3 T^2 + c_4 T^3 + c_5 x + c_6 x T + c_7 x T^2 + c_8 x T^3$$
$$+ c_9 x^2 + c_{10} x^2 T + c_{11} x^2 T^2 + c_{12} x^2 T^3 + c_{13} x^3 + c_{14} x^3 T$$
$$+ c_{15} x^3 T^2 + c_{16} x^3 T^3$$

where x is sensor output signal and T is temperature.

An example of Design 2 microbend sensor response data for the operational and high-temperature tests is shown in Figure 16. In this figure, the data for the decreasing temperature sequence runs was not plotted for pressures other than zero for clarity. The Design 2 sensor response exhibited a much smaller zero pressure

shift with temperature than that of Design 1. The Design 2 response data was similar to the corrected Design 1 data as previously shown in Figure 9.

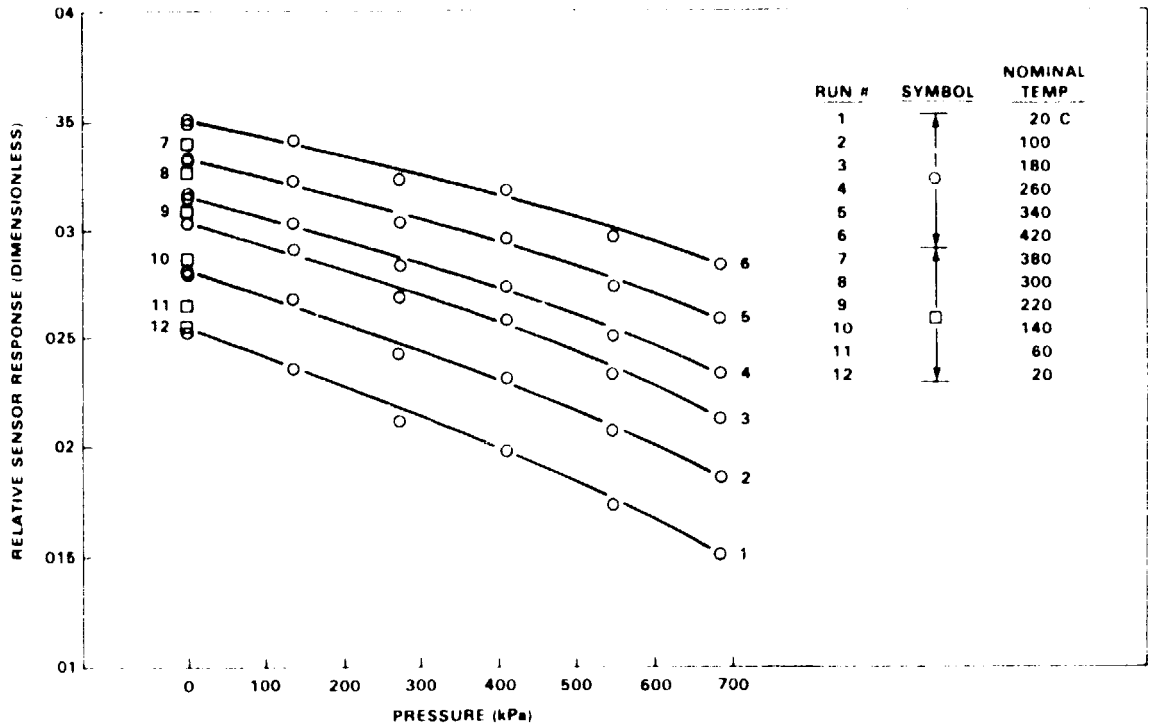

Figure 16. Typical microbend sensor response data -- Design 2.

The results of the Design 2 data curve fits are shown in Tables 2 and 3. Table 2 lists the 95% confidence level deviation of input pressure from the pressure calculated from the individual calibration equations for each nominal temperature for full-scale response.

Table 2

MICROBEND SENSOR RESPONSE -- DESIGN 2
(Results of pressure curve fits only)

Run No.	Full-Scale Error	Run No.	Full-Scale Error
T1	3.1	T7	5.3
T2	4.8	T8	2.0
T3	3.3	T9	2.0
T4	4.8	T10	2.3
T5	5.4	T11	0.3
T6	9.1	T12	1.1

Table 3

MICROBEND SENSOR RESPONSE -- DESIGN 2
(Results of combined temperature and pressure curve fits)

Number of Parameters Used	Overall Full-Scale Error
8	3.73%
10	3.64%
15	3.73%

REGRESSION DATA FOR 10-PARAMETER CURVE FIT

Variable	Regression Coefficient	Variable	Regression Coefficient
Intercept	$-2.33286\ 10^{2}$	xT3	$1.66907\ 10^{-3}$
T	-4.24635	x2	$-1.177046\ 10^{7}$
x	$2.0075\ 10^{5}$	x2T	$-9.03524\ 10^{3}$
T2	$3.43232\ 10^{-3}$	x3	$1.62064\ 10^{8}$
T3	$-4.4917\ 10^{-5}$	x3T2*	$-2.67319\ 10^{2}$
xT	$5.11445\ 10^{2}$		

* For example, where $x3T2 = x^{3}T^{2}$

In Table 2, the relative magnitude of the full-scale error is increased due to the limited number of data points used for the curve fits. However, most of the increase in error with temperature, noted in the Design 1 data, has been eliminated.

Table 3 lists the 95% confidence level deviation of input pressure from the pressure calculated from the overall temperature compensated calibration equation for several curve fits. Not all of the terms in the calibration equation were significant; the stepwise regression analysis eliminated terms of low tolerance.

The average of the individual curve fit error was about 3.6% which is about equal to the overall curve fit error. This shows that the sensor temperature response is predictable and, thus compensatable.

4. DEVELOPMENT OF PHASE SENSITIVE SENSOR

The development of the Phase Sensitive Optical Diaphragm Deflection Sensor (phase sensitive sensor) included the sensor design, the sensor module design, and the sensor evaluation by a series of specified tests.

4.1 SENSOR DESIGN

The sensor design was based on the objectives of using a non-metallic diaphragm to eliminate or reduce creep and hysteresis, and to meet the requirements of temperature, pressure, and vibration response. Design constraints include operation to 540°C, response to differential pressure of ±690 kPa full scale, ability to withstand 3X full-scale overpressure, and minimal vibrational response from 50 to 2500 Hz.

The basic module design was similar to that used for the microbend sensor discussed eariler in Section 3.1.1. For the phase sensitive sensor, the module consisted of a fused silica base used to secure the end of a bundle of optical fibers, and a fused silica diaphragm to act as a reflector.

The phase sensitive sensor is illustrated in Figure 17. A bundle of single-mode optical fibers was cemented into a central hole in the base plate. Both the fiber leads and a thermocouple to measure sensor temperature were inserted through the stainless steel tubes of the base flange. Multiple single-mode fibers were used to provide redundance in case of failure of any one fiber, and to provide a choice of that fiber with optimum response to diaphragm deflection.

This sensing method can be explained as follows: Light propagating in one of the single-mode fibers is partially reflected at the fiber end surface-air interface (reference light signal). The transmitted beam is partially reflected from the air-diaphragm surface interface. A portion of this reflected beam couples back into the fiber (deflection light signal) and both reflected components propagate

back to the fiber input end where they are mixed on a photodiode. This sensor acts as a two-beam interferometer if the surfaces are uncoated. To avoid multiple fringe ambiguity at full-scale pressure, the diaphragm deflection should be less than $\lambda/8$. Based on the model of a clamped diaphragm, the required diaphragm thickness was determined to be 14 mm.

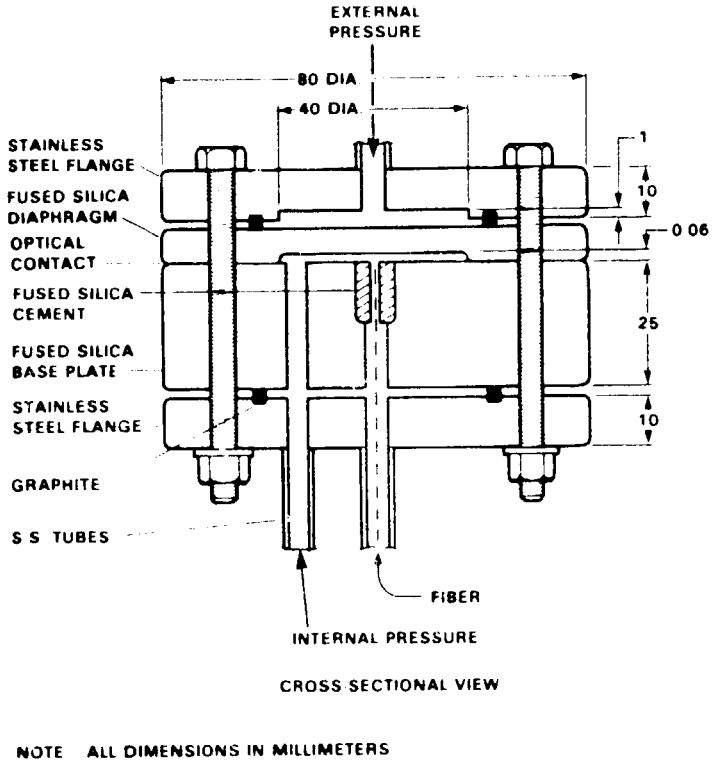

Figure 17. Phase sensitive sensor.

The photodiode output signal is proportional to the optical phase difference between the two reflected components. Since environmental perturbations of the fiber affect both reflected components identically, phase shifts from these perturbations cancel. Phase shifts are imposed on the light that exits the fiber; this phase difference is given by:

$$\Delta\phi = \frac{2\pi}{\lambda}(2nh) + \psi_2 - \psi_1$$

where:

n = Refractive index of air (or other gas) in the gap between the diaphragm and base plate

h = Gap height of diaphragm from base plate

ψ_2 = Phase shift on reflection from diaphragm

ψ_1 = Phase shift on reflection from fiber surface

λ = Wavelength of source in vacuum

The primary sensor response is generated from the change in h with pressure. Other possible sources of sensor response are changes in n, ψ_2, and ψ_1.

The pressure seals for both internal and external pressure were provided by graphite gaskets between the steel flanges and the fused silica components. Sealing pressure was provided by a suitable means such as bolts between the end flanges. An exploded view of the sensor is shown in Figure 18 for the steel flange test configuration.

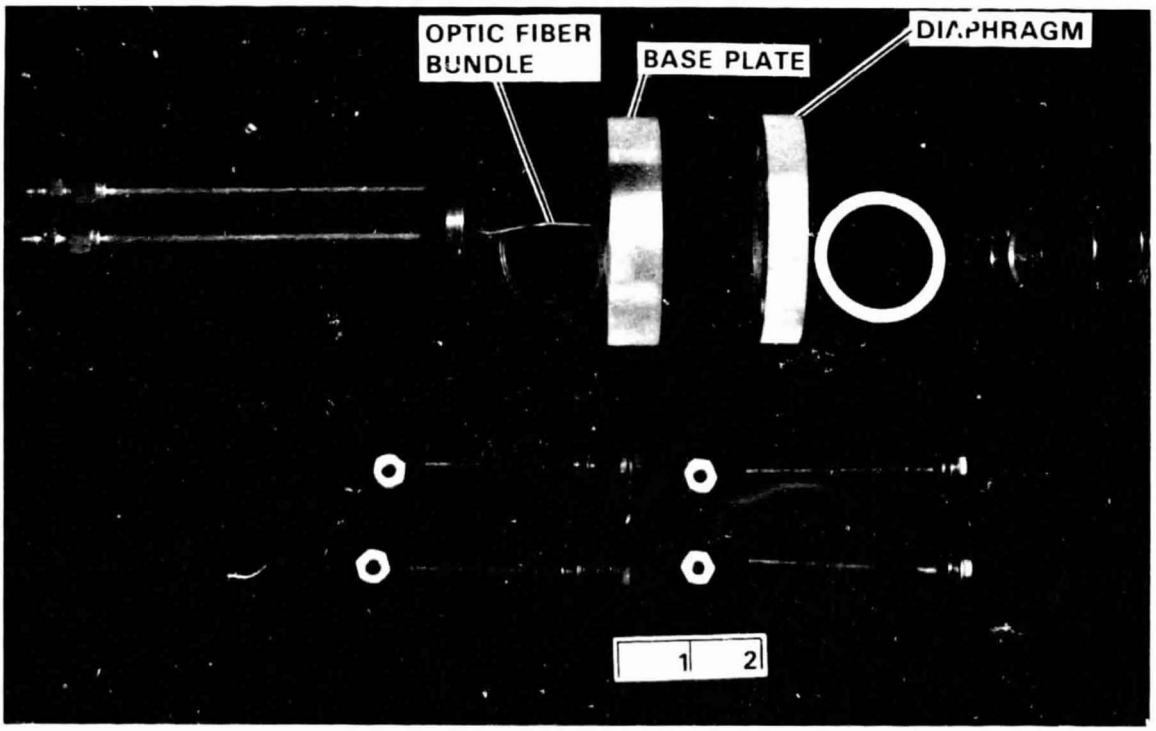

Figure 18. Phase sensitive sensor -- exploded view.

4.2 SENSOR EVALUATION

The phase sensitive sensor was evaluated by a series of specified tests to determine the pressure, temperature, overpressure, and vibration response of the sensor. Sensor evaluation can be summarized as follows:

- The sensor response was approximately a cosine-squared function of pressure.
- The sensor exhibited high sensitivity to diaphragm deflection.
- Response to pressure changes was rapid.
- The sensor was insensitive to vibration for 50 Hz to 2500 Hz.
- The sensor withstood 3X full-scale pressure.
- The sensor module was capable of 540°C operation.
- The single-mode optical fibers were capable of 540°C operation.
- The sensor response, as tested, passed through multiple fringes upon full-scale external or internal pressurization.
- The sensor response was different for internal pressurization than for external pressurization.

4.2.1 Operational and High-Temperature Evaluation

The purpose of the operational and high-temperature tests was to characterize the sensor response for a sequence of differential pressures from -690 kPa (internal) to +690 kPa (external). The phase sensitive sensor setup for testing is shown in Figure 19. The output of the laser diode is spliced to a 3 dB single-mode coupler. One of the coupler outputs is precisely positioned to feed through index matching fluid to the single-mode fiber in the sensor. The other coupler output was not used and led to an optical sink consisting of a drop of index matching fluid. The return optical fiber from the coupler goes to a single silicon detector. The detector senses the interference of light reflected from the opposite end of the optical fiber in the sensor and the light reflected from the sensor diaphragm. The output of the electronics goes to the A/D converter for data processing and storage.

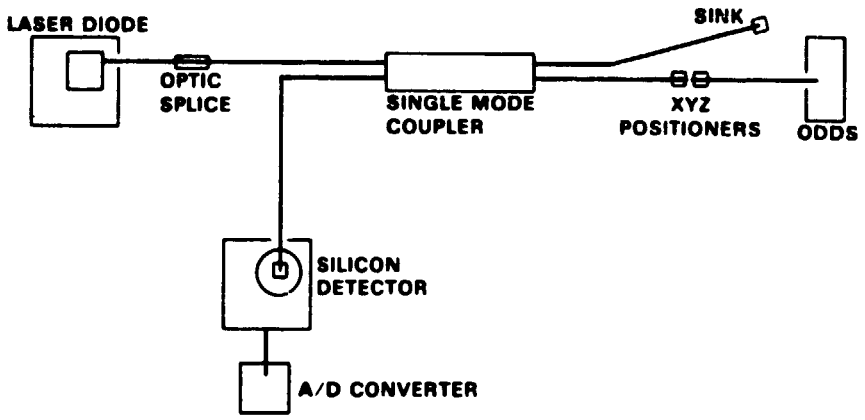

Figure 19. Phase sensitive sensor system block diagram.

The test setup was similar to that shown previously in Figure 8; however, the sensor was in a pressure chamber located in the furnace. Multiple fringes were observed upon both positive and negative pressurization. The sensor characterization data runs were then curve-fit to the expression:

$$y = B(1)\left\{\cos^2\left(\frac{\pi}{B(2)}\left[x - B(3)\right]\right)\right\} + B(4)$$

where:

y = Predicted sensor response

B(1) = Scale factor

B(2) = Fringe period factor

B(3) = Fringe phase factor

B(4) = Signal offset

x = Pressure

The change in the index of refraction upon internal pressurization required separate curve fits for internal and exernal pressure response. Figure 20 shows the curve fit for positive pressure at about 120°C. The results of curve-fit data is shown in Table 4. The % error of individual runs was not meaningful due to the multiple fringe ambiguity. Also, the overall % error was not meaningful due to multiple fringe ambiguity for a given temperature, and phase ambiguity between runs at different temperature. The assumption of a clamped diaphragm was

incorrect to predict the desired deflection; thus, a thicker diaphragm would be required to provide a full-scale deflection less than one-half a wavelength.

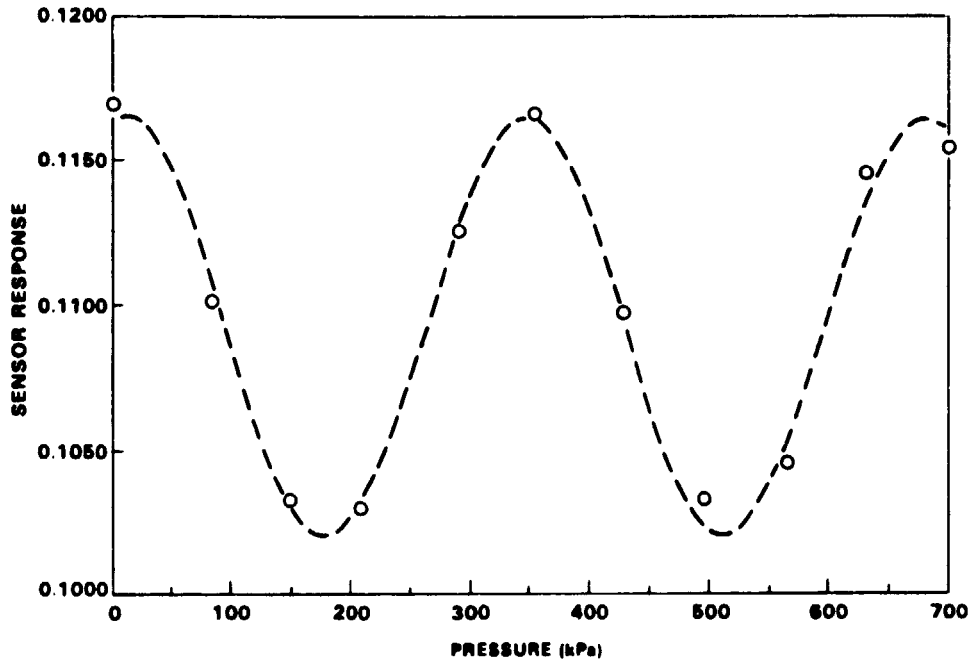

Figure 20. Phase sensitive sensor -- Run 3 response.

Table 4

PHASE SENSITIVE SENSOR
PHASE 1 CALIBRATION DATA

Calib. Run	Nominal Temp °C	Pressure kPa	ESS	SD	Sensor Span Per Fringe	No. Fringes Per 690 kPa
1	24	External	$0.8168\ 10^{-5}$	$1.668\ 10^{-3}$	$0.1765\ 10^{-1}$	3.96
2	24	Internal	$0.7809\ 10^{-5}$	$1.141\ 10^{-3}$	$0.1577\ 10^{-1}$	5.15
3	120	External	$0.3944\ 10^{-5}$	$0.811\ 10^{-3}$	$0.1434\ 10^{-1}$	4.13
4	220	External	$0.3883\ 10^{-5}$	$0.804\ 10^{-3}$	$0.8967\ 10^{-2}$	4.48

ESS = Estimated Sums of Squares; SD = Standard Deviation

4.2.2 Vibration Tests

The vibration test objectives were to observe and record any mechanical resonances associated with the sensing device. These tests were similar to those previously reported in Section 3.2.2 for the microbend sensor. An example of test data is shown in Figure 21 where 1% full-scale response corresponds to 0.3 millivolt. Essentially no response to vibration was observed over the frequency range of the tests.

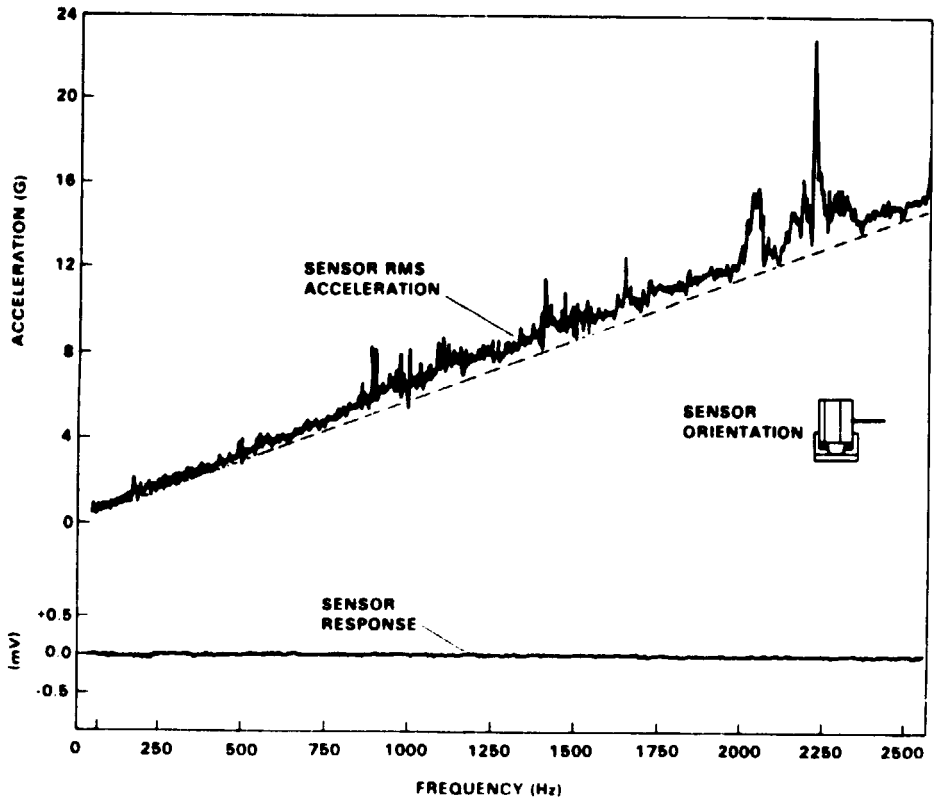

Figure 21. Typical phase sensitive sensor vibration results.

4.2.3 Overpressure Tests

The overpressure tests were to verify that the phase sensitive sensor would withstand three times full-scale pressure without failure and to note any changes in the sensor response with respect to a baseline calibration equation.

The overpressure tests were similar to those reported earlier in Section 3.2.3 for the microbend sensor. A series of additional calibration runs were conducted

along with the overpressure and standard static calibration runs. Calibration run data is shown in Table 5. For each static calibration, an estimate of the 95% confidence level deviation of the input pressure from the pressure calculated from the calibration equation from a baseline static calibration was obtained as a percentage of full-scale pressure.

Table 5

PHASE SENSITIVE SENSOR
PHASE 2 CALIBRATION DATA

Calib. Run	Nominal Temp °C	Pressure kPa	ESS	SD	Sensor Span Per Fringe	No. Fringes Per 690 kPa
1	24	External	$0.4938\ 10^{-3}$	$8.399\ 10^{-3}$	0.2649	2.19
2	24	Internal	$0.1350\ 10^{-2}$	$13.887\ 10^{-3}$	0.2553	3.78
3	24	External	$0.7429\ 10^{-3}$	$10.302\ 10^{-3}$	0.2705	2.22
4	24	Internal	$0.1211\ 10^{-2}$	$13.153\ 10^{-3}$	0.2535	3.77
5	24	External	$0.8809\ 10^{-3}$	$11.218\ 10^{-3}$	0.2708	2.25
6	24	Internal	$0.9475\ 10^{-3}$	$11.634\ 10^{-3}$	0.2534	3.74

ESS = Estimated Sums of Squares; SD = Standard Deviation

The results of the overpressure test sequence are shown in Figure 22. The overpressure static calibration data was compared to three baseline calibrations. The change in the predicted error was attributed to an uncompensated phase shift with time during the tests. This uncompensated phase shift was in turn attributed to micromotion of the fiber optic bundle with respect to the fused silica reference platform due to differential expansion effects. With an improved method of securing the fiber optic bundle and pressure sealing the module, the sensor should be insensitive to overpressure excursions.

Although the phase sensitive sensor performed well, it had the following problems which made the overall performance inferior to the microbend sensor: securing fiber ends, time dependent drift, different response for internal and external pressure, and diaphragm deflection greater than one wavelength which led to multiple fringe ambiguity problems.

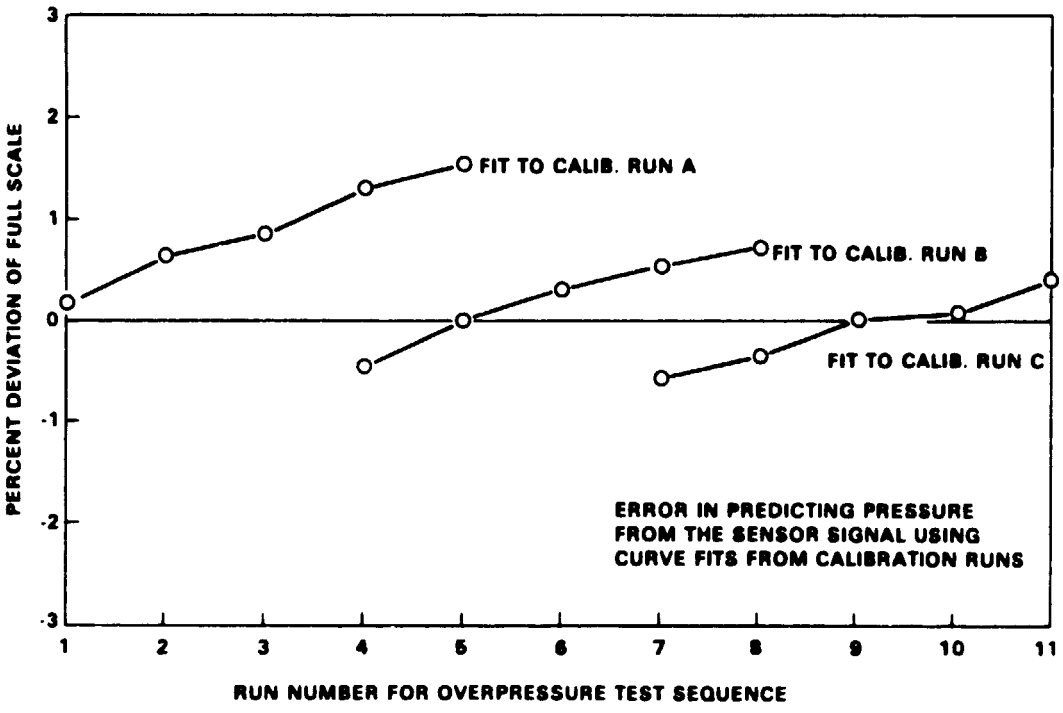

Figure 22. Analysis of phase sensitive sensor response during overpressure test sequence.

5. OTHER SENSORS INVESTIGATED

Nine sensors were investigated in this project. Of these, five were recommended for initial development and testing. The microbend sensor and the phase sensitive sensor were previously discussed in Sections 3 and 4. In this section (Section 5) the two-fiber transmission sensor, the cantilever slope sensor, and the photoelastic sensor will be briefly discussed.

5.1 TWO-FIBER TRANSMISSION SENSOR

The two-fiber transmission sensor sensed diaphragm deflection via a light intensity change. Light coupled into receive optical fibers changed with translation of a transmit optical fiber attached to the diaphragm, when both transmit and receive fibers were nearly aligned. Thus, the change in the light intensity in the receive fibers, as a result of the change in coupling, was used as a measure of translation caused by diaphragm deflection.

5.1.1 Sensor Design

The two-fiber transmission sensor and associated components are shown in Figure 23. Multimode optical fibers were cemented into grooves ground along the ends of two pedestals. One pedestal was located in the center of the diaphragm; the second pedestal was optically contacted to the fused silica base plate. The diaphragm was optically contacted to the base plate around an outer annulus. The optical fiber leads and thermocouple to measure sensor temperature were inserted through metal tubes on the sensor metal end plate. The modified test setup was used for this test; end plates were used with graphite gaskets to provide the pressure seals.

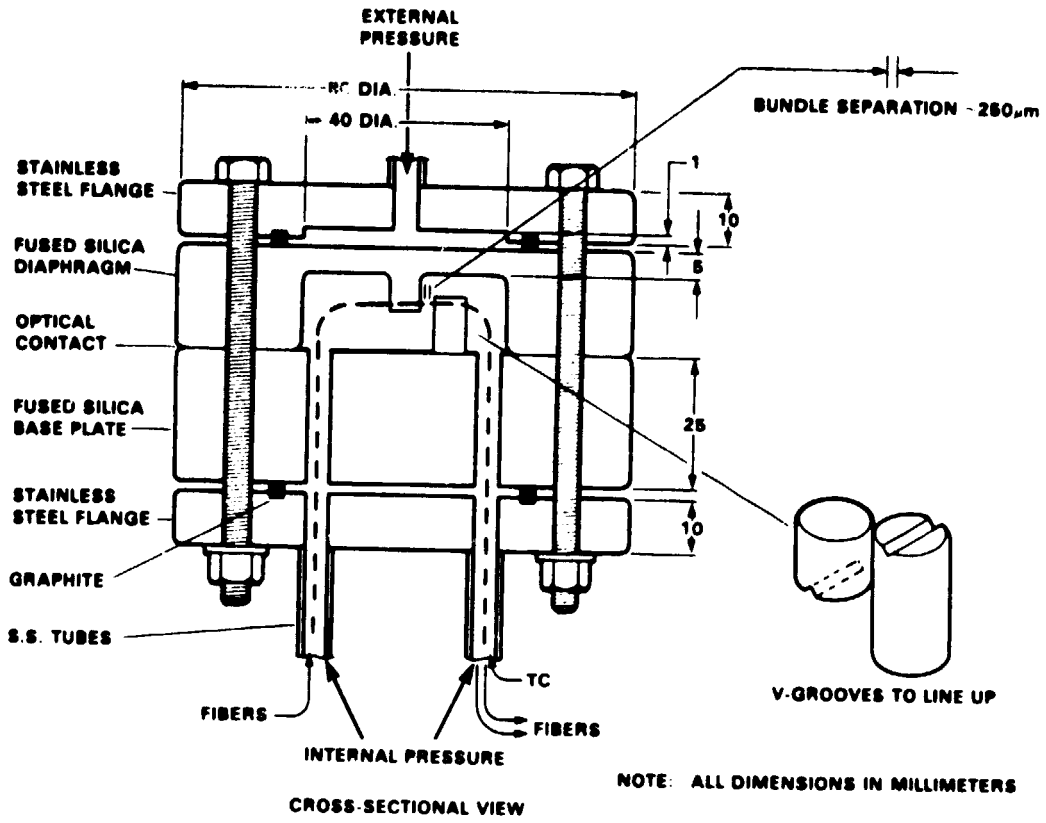

Figure 23. Two-fiber transmission sensor.

Multiple fibers were cemented into the grooves on each pedestal using fused silica cement. This approach provided:

1) Redundancy in case of failure of any fiber

2) Non-critical alignment requirements for the two pedestals during assembly

3) Multiple transmit and receive fibers from which to choose those which provided optimum response to concave and/or convex diaphragm deflection

With the light-transmitting fiber mounted on the diaphragm pedestal, deflection of the diaphragm caused translation of the fiber axis along the y-direction. The motionless receive fibers on the reference platform pedestal were axially aligned with the transmit fiber. When the transmit fiber moved with diaphragm deflection, the amount of optical power coupled into the receive fibers changed.

For this sensor, a multimode, high-temperature optical fiber with a numerical aperture of about 0.65 and a core-to-clad area ratio of about 25:1 was required to achieve the best sensitivity possible. The best available optical fiber meeting those requirements was limited in operating temperature to about 400°C. As a result, the sensor was not repeatable at or above about 400°C.

5.1.2 Operational and High-Temperature Evaluation

The two-fiber transmission sensor setup for testing is shown in Figure 24. The laser diode source was coupled to a selected transmit fiber. The two selected receive fibers were coupled to the dual photodetector and associated electronics. The test sequence was similar to that described for the microbend sensor in Section 3.

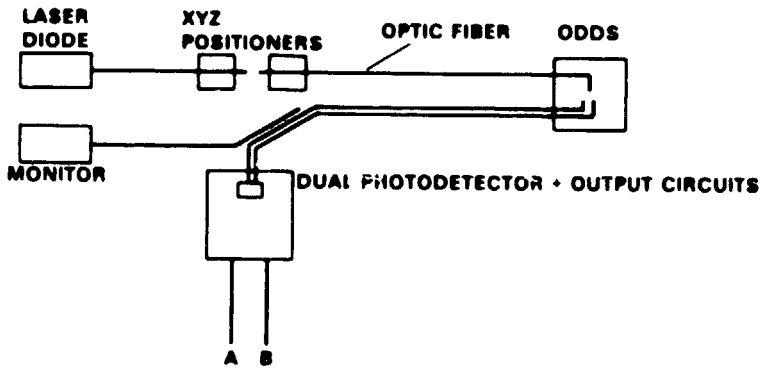

Figure 24. Two-fiber transmission sensor system block diagram.

The sensor response was approximately linear with pressure for both internal and external pressurization. The sensor response was relatively weak however, being about a factor of 5 less sensitive than the microbend sensor. This relative sensitivity was determined by comparing the slope of pressure response for both the two-fiber and microbend sensors. The major problems with this sensor, as tested, were the limitations imposed by the best available optical fiber. The light transmission characteristics of the fiber in the test configuration were a function of temperature and were limited to about 400°C. Further, the fiber differential expansion, with respect to the fused silica module material, caused degradation of the cemented fiber bundle ends with repeated temperature cycles to 540°C. Thus, a large numerical aperture optical fiber with improved high-temperature performance, and an improved method of securing the fiber ends to fused silica are required to make this sensor rugged, reliable, and repeatable.

5.2 CANTILEVER SLOPE SENSOR

The Cantilever Slope Optical Diaphragm Deflection Sensor (cantilever slope sensor) was based on the principle of differential collection of light from a reflector that was subject to tilting. A change in the reflector tilt angle selectively increased the light coupled into some fibers and decreased the light coupled into other fibers. This differential light coupling was used as a measure of reflector tilt corresponding to diaphragm deflection.

5.2.1 Sensor Design

The cantilever slope sensor and its components are shown in Figure 25. In this configuration, the diaphragm deflects a cantilever beam that acts as the reflective surface. The slope of the cantilever was greater than the slope on the diaphragm by a factor equal to the ratio of the diaphragm radius to the length of the cantilever. The cantilever was therefore made as short as practicable. It was anticipated that a mechanical gain of at least 5 could be achieved.

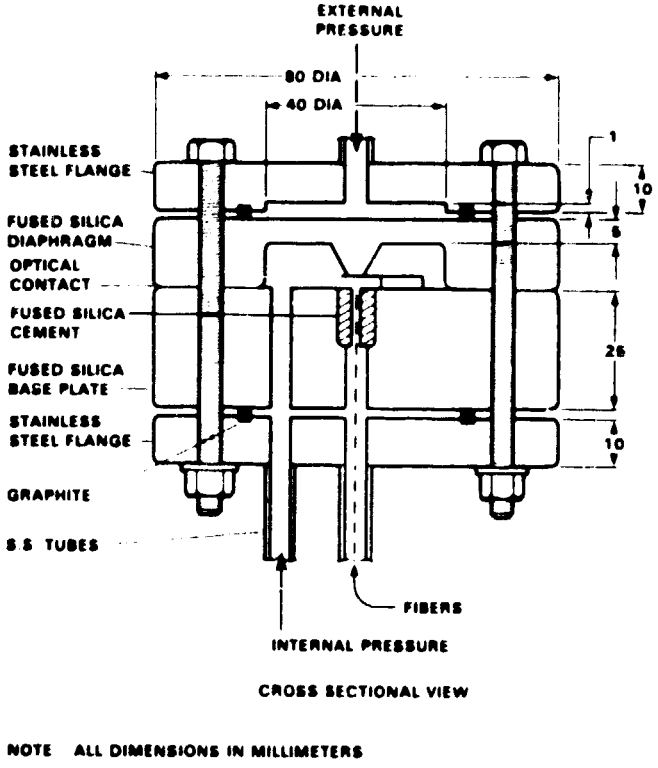

Figure 25. Cantilever slope sensor.

A bundle of fibers was cemented into the base plate. From this bundle, one fiber was used as the transmitter; two or more fibers were used as the receive fibers.

5.2.2 Operational and High-Temperature Evaluation

The cantilever slope sensor setup for testing is shown in Figure 26. A laser diode was coupled to the transmit fiber. The receive fibers were coupled to a dual photodiode and associated electronics. To achieve the best possible sensitivity, high-temperature fibers satisfying the requirements of numerical aperture of about 0.65 and a core-to-clad area ratio of about 25:1 were used for the tests. However, these optical fibers limited the testing to an upper temperature of about 400°C; the fibers also were difficult to cement or secure in a bundle due to differential expansion effects with respect to fused silica over the temperature range of operation. These problems were similar to those encountered with the two-fiber transmission sensor described earilier in Section 5.1.1.

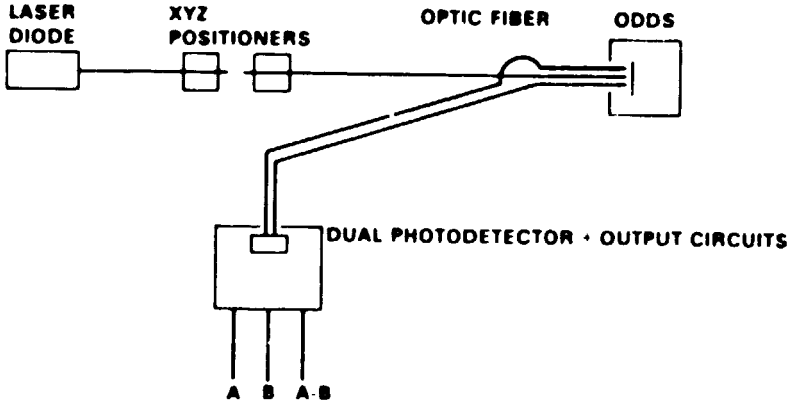

Figure 26. Cantilever slope sensor system block diagram.

The cantilever slope sensor response was approximately linear with pressure. However, the signal change with cantilever deflection was greater than that due to slope change. Thus, the differential sensitivity was unsatisfactory. The sensor response also exhibited excessive scatter, which appeared to be due to nonuniform relative motion or slippage between the diaphragm "tooth" and the cantilever (see Figure 25). Thus, for this sensor, a large numerical aperture fiber with improved high-temperature performance, an improved method of securing the fiber ends, and an improved cantilever mechanical design are required to make this sensor reliable, repeatable, and rugged.

5.3 PHOTOELASTIC SENSOR

The Photoelastic Optical Diaphragm Deflection Sensor (photoelastic sensor) was based on measurement of the change in stress-induced birefringence in a single mode optical fiber clamped between a pedestal and the diaphragm. The relative change in birefringence was caused by changes in pressure on the diaphragm which caused changes in stress on the clamped fiber.

5.3.1 Sensor Design

The photoelastic sensor and associated components are shown in Figure 27. The fused silica sensor module was similar to that used for the other sensors.

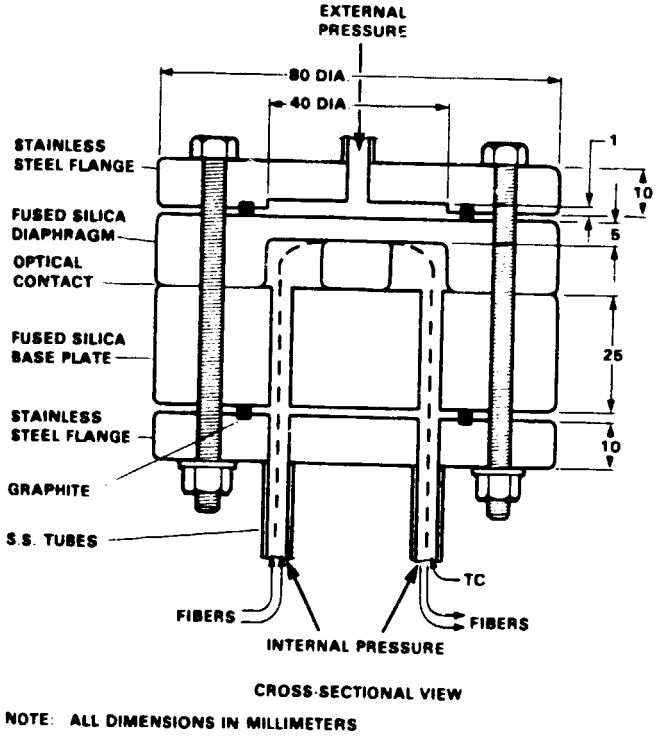

Figure 27. Photoelastic sensor.

A single mode, polarization preserving optical fiber was squeezed between a rigid pedestal and the diaphragm. Both the pedestal (at its base) and the diaphragm were optically contacted to the fused silica base plate. The optical fiber leads and thermocouple to measure sensor temperature were inserted through the metal tubes on the sensor metal end plate containing the graphite pressure seal gasket.

5.3.2 Operational and High-Temperature Evaluation

The photoelastic sensor was tested using the associated components shown in Figure 28. Separate tests as a function of temperature, and pressure at elevated temperature showed that the desired birefringence response could be obtained. However, the sensor was not tested in the fused silica pressure module configuration due to the lack of an optic fiber that would withstand pressurization without fracture or deformation of the fiber coating. For proper operation of this sensor, a single mode, polarization preserving optical fiber is needed with a coating that has hardness comparable to fused silica to prevent deformation. Such an optic fiber was not available for the testing of the assembled photoelastic sensor module.

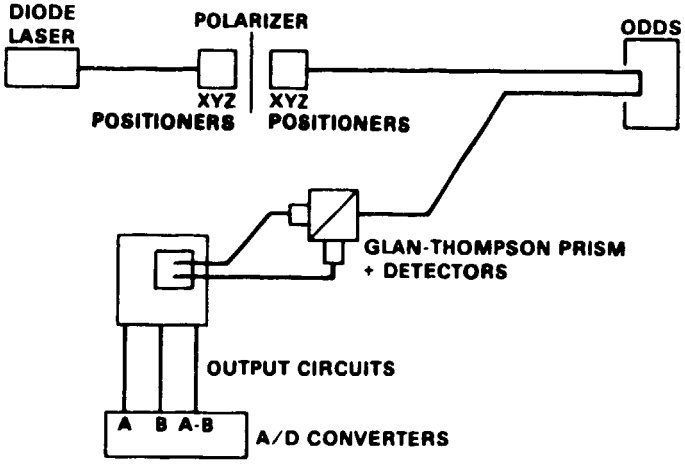

Figure 28. Photoelastic sensor system block diagram.

6. DISCUSSION OF RESULTS

The results of this project and the degree to which the objectives were met were a direct function of the project constraints. Thus, the project will be discussed in terms of the effect of the constraints on the results.

The primary constraints for the sensor module design were the use of a non-metallic diaphragm, operation with either internal or external pressure to 690 kPa, able to withstand 3X full-scale overpressure, and operation in the temperature range of ~20° to 540°C. As most high-temperature, non-metallic materials are brittle and must be limited in tension, the design result was a thick diaphragm with little deflection upon pressurization. The fused silica modules used in the sensors satisfied the pressure and temperature requirements. However, they presented problems in pressure sealing, attachment to other components was difficult, residual stress problems were difficult to avoid, and the fused silica was prone to fracture at points of inadvertent high stress during testing. These problems required the redesign of the module for the Phase 2 sensor systems tests. The redesigned sensor module, however, retained the thick diaphragm with its small deflection with applied pressure.

The constraints for the sensing system included the use of an optical method to sense diaphragm deflection, the sensing system was to be non-metallic, and practical considerations required the use of commercially available optical fibers and high-temperature cements. As the diaphragm deflections were small, the optical sensing methods were required to measure $\sim 10^{-8}$ m deflections. The microbend, phase sensitive, and photoelastic sensing methods were sufficiently sensitive for these small deflections; the two-fiber transmission and the cantilever slope sensing methods possessed only marginal sensitivity for these small deflections. It should be noted that a relaxation of the overpressure requirements would allow a two- to five-fold increase in the diaphragm deflection and would allow the use of less sensitive sensing methods.

Using commercially available optical fibers and high-temperature cements restricted the useful temperature range for several of the sensors. Although fibers that will operate at 540°C are available, the optical sensing methods required fibers with specific optical parameters such as non-standard numerical aperture. Optical fibers meeting the sensing method requirements were often limited in their temperature range. This was the case for the fibers used in the microbend, two-fiber transmission, and cantilever slope sensors.

Sensors with a continuous optical fiber, such as the microbend and the photoelastic sensors, were advantageous in that the fiber needed only to be constrained to the sensing region. Sensors such as the phase sensitive, two-fiber transmission, and cantilever slope required that the ends of fibers or fiber bundles be secured in the sensor. Instability resulted when commercially available fibers and cements were used because these materials invariably exhibited a mismatch in thermal expansion between the optical fibers and the fused silica module. Repeated temperature cycles to 540°C tended to loosen the fibers or fiber bundles and eventually allow micro-movement of the fibers with respect to the module. Due to the small diaphragm deflection and the high sensitivity of the optical sensing methods, any relative movement of the fibers or the sensor module components caused a change (gain, offset, or both) in the sensor signal. Thus, second-order effects were often important. For example, this was seen in the zero shift due to changes in the sealing pressure for the Design 1 module.

The constraints of operation at peak velocity of 12.7×10^{-3} m/second (0.5 inch/second) and frequency response to 2 kHz required support of the fibers to eliminate resonant mode and sufficiently fast electronics. Due to the high sensitivity of the optical sensing methods and the limited signal-to-noise ratio, a longer time constant on the sensor electronics would be advantageous to reduce data scatter.

The microbend optical diaphragm deflection sensor met most of the requirements and objectives of the project. The microbend sensor exhibited high sensitivity to diaphragm deflection; the response was approximately linear with pressure from -690 kPa (internal pressure) to +690 kPa (external pressure). The sensor response to pressure change was rapid, it was insensitive to vibration from 50 to 2500 Hz, and it withstood 3X full-scale pressure. The sensor module was capable of 540°C

operation; the best available high-temperature fiber produced repeatable response to about 450°C. The Design 2 module reduced the zero offset with temperature. The Design 2 test data showed that many of the problems associated with Design 1 had been eliminated. The Design 2 microbend sensor data as a function of pressure and temperature was self-consistent and allowed an overall curve fit with a deviation that was close to the project objective of acceptable level of ~3%. The Design 2 data still showed hysteresis that is believed to be associated with the interaction of the sensor microbend "teeth" and the aluminum coating on the optic fiber. It is believed that this hysteresis could be reduced or eliminated by a combination of larger diaphragm deflection, smoother finish on the microbend "teeth", and an improved coating on the optical fiber.

7. SUMMARY OF RESULTS AND CONCLUSIONS

The objective of this project was to study, design, develop, fabricate, assemble, test, evaluate, and document optical diaphragm deflection sensors which:

- Accurately measure diaphragm deflection due to a pressure difference across its surface
- Meet the operational and environmental requirements of pressure measurement systems for high-performance aircraft
- Take advantage of current technology in optics, electronics, and material science

The project results showed that a high-temperature pressure sensor based on a non-metallic (ceramic or glass diaphragm) is feasible. Glass diaphragms, such as fused silica, are limited in their allowable deflection and thus require sensitive sensing methods. The microbend sensor, which was based on the attenuation of light transmitted through the core of an optical fiber caused by periodic bending of the fiber, was sufficiently sensitive to meet the project objectives. The Design 2 microbend sensor exhibited the desired sensitivity and stability as a function of temperature and pressure to be used as the basis for a compensatable sensor.

The present limitations on the microbend sensor performance are due to the temperature limits on suitable commercially available optical fibers, the available coatings on such fibers, and pressure sealing of the sensor module for differential pressures.

Ceramic/glass diaphragms and/or optical methods for detecting diaphragm deflection in a high-temperature pressure sensor should also be considered for applications such as advanced energy conversion systems, in addition to high-performance aircraft. Such applications with reduced or different design constraints may be directly amenable to solution by state-of-the-art components and sensing methods such as those investigated in this project.

Improvements in commercially available optical fiber characteristics such as maximum operating temperature and surface coating are required. Optical fiber manufacturers should be encouraged to develop fibers with improved high-temperature characteristics.

1. Report No.	2. Government Accession No.	3. Recipient's Catalog No.
NASA CR-175008		

4. Title and Subtitle

DEVELOPMENT OF OPTICAL DIAPHRAGM DEFLECTION SENSORS, FINAL REPORT

5. Report Date

JUNE 1985

6. Performing Organization Code

505-40-14

7. Author(s)

W. L. Ghering, D. Varshneya, L. A. Jeffers, R. T. Bailey, and J. W. Berthold

8. Performing Organization Report No.

RDD:85:4101-12-01:01

10. Work Unit No.

9. Performing Organization Name and Address

THE BABCOCK & WILCOX COMPANY
Research and Development Division
1562 Beeson Street, Alliance, Ohio 44601

11. Contract or Grant No.

NAS3-23712

13. Type of Report and Period Covered

CONTRACTOR REPORT

12. Sponsoring Agency Name and Address

NATIONAL AERONAUTICS AND SPACE ADMINISTRATION
Washington, D C. 20546

14. Sponsoring Agency Code

15. Supplementary Notes

John P. Barranger, Project Manager
NASA Lewis Research Center, Cleveland, Ohio 44135

16. Abstract

The objective of this project was to develop high-temperature pressure sensors using non-metallic components and optical sensing methods. The sensors were to operate over a temperature range from room temperature (~20°C) to 540°C, to respond to internal pressure up to 690 kPa, to respond to external pressure up to 690 kPa, and to withstand external overpressure of 2070 kPa. Project tasks included evaluating sensing techniques and sensor systems. These efforts included materials and sensing method selection, sensor design, sensor fabrication, and sensor testing. Sensors were tested as a function of temperature, pressure, overpressure, and vibration. The project results showed that high-temperature pressure sensors based on glass components and optical sensing methods are feasible. The microbend optical diaphragm deflection sensor exhibited the required sensitivity and stability for use as a pressure sensor with temperature compensation. For the microbend sensor, the 95% confidence level deviation of input pressure from the pressure calculated from the overall temperature-compensated calibration equation was 3.7% of full scale. The limitations of the sensors evaluated were primarily due to the restricted temperature range of suitable commercially available optical fibers and the problems associated with glass-to-metal pressure sealing over the entire testing temperature range.

17. Key Words (Suggested by Author(s))	18. Distribution Statement
Pressure Measurement, High Temperature, Fiber Optic Sensors, Fused Silicon Devices, Diaphragm Pressure Transducers, Aircraft Engine Sensors	FOR GENERAL RELEASE

19. Security Classif. (of this report)	20. Security Classif. (of this page)	21. No. of pages	22. Price*
UNCLASSIFIED	UNCLASSIFIED	62	

*For sale by the National Technical Information Service, Springfield, Virginia 22161